Progress in Oceanography 81 (2009) 223–236

Contents lists available at ScienceDirect

Progress in Oceanography

journal homepage: www.elsevier.com/locate/pocean

Fronts in Large Marine Ecosystems

Igor M. Belkin [a,*], Peter C. Cornillon [a], Kenneth Sherman [b]

[a] Graduate School of Oceanography, University of Rhode Island, 215 South Ferry Road, Narragansett, RI 02882, USA
[b] NOAA/NMFS/NEFSC, Narragansett Laboratory, 28 Tarzwell Drive, Narragansett, RI 02882, USA

ARTICLE INFO

Available online 23 April 2009

ABSTRACT

Oceanic fronts shape marine ecosystems; therefore front mapping and characterization are among the most important aspects of physical oceanography. Here we report on the first global remote sensing survey of fronts in the Large Marine Ecosystems (LME). This survey is based on a unique frontal data archive assembled at the University of Rhode Island. Thermal fronts were automatically derived with the edge detection algorithm of Cayula and Cornillon (1992, 1995, 1996) from 12 years of twice-daily, global, 9-km resolution satellite sea surface temperature (SST) fields to produce synoptic (nearly instantaneous) frontal maps, and to compute the long-term mean frequency of occurrence of SST fronts and their gradients. These synoptic and long-term maps were used to identify major quasi-stationary fronts and to derive provisional frontal distribution maps for all LMEs. Since SST fronts are typically collocated with fronts in other water properties such as salinity, density and chlorophyll, digital frontal paths from SST frontal maps can be used in studies of physical–biological correlations at fronts. Frontal patterns in several exemplary LMEs are described and compared, including those for: the East and West Bering Sea LMEs, Sea of Okhotsk LME, East China Sea LME, Yellow Sea LME, North Sea LME, East and West Greenland Shelf LMEs, Newfoundland–Labrador Shelf LME, Northeast and Southeast US Continental Shelf LMEs, Gulf of Mexico LME, and Patagonian Shelf LME. Seasonal evolution of frontal patterns in major upwelling zones reveals an order-of-magnitude growth of frontal scales from summer to winter. A classification of LMEs with regard to the origin and physics of their respective dominant fronts is presented. The proposed classification lends itself to comparative studies of frontal ecosystems.

1. Introduction

An oceanic front is a narrow zone of enhanced horizontal gradients of water properties (temperature, salinity, nutrients, etc.) that separates broader areas with different water masses or different vertical structure (stratification) (Belkin, 2002). Fronts are often described as discontinuities because of their abrupt nature. Fronts occur on a variety of length scales, from a few meters up to many thousands of kilometers. Fronts can be short-lived (days), although most fronts are quasi-stationary and seasonally persistent; prominent fronts are present year-around. Cross-frontal differences in SST and sea surface salinity can be as large as 10–15 °C and 2–3 parts per thousand (ppt), respectively; typical differences are 2–5 °C and 0.3–1.0 ppt. The vertical extents of fronts vary from a few meters to more than a kilometer, with major fronts reaching the open ocean bottom at depths exceeding 4 km.

Various physical processes can form diverse fronts, including estuarine, plume, and coastal buoyancy current fronts; tidal mixing fronts; mid-shelf fronts; shelf-slope/shelfbreak fronts; coastal, topographic, and equatorial upwelling fronts; western and eastern boundary current fronts; subtropical convergence fronts; marginal ice zone fronts, and water mass fronts (Belkin, 2002). These fronts also have chemical and biological manifestations. As a rule, a front in one property can be detected in other properties. For example, temperature fronts are almost always associated with salinity fronts. Such thermohaline fronts are often accompanied by density fronts since sea water density is a function of temperature, salinity, and pressure (depth). Major thermohaline fronts are associated with fronts in other properties, such as nutrients, ocean color, chlorophyll, and turbidity. The concurrent physical, chemical, and biological manifestations of the same front are typically collocated, although relatively minor spatial offsets have been observed between locations of the same fronts in different properties. This well-established collocation of various facets of the same front provides ample evidence strongly supporting satellite observations of sea surface temperature (SST) fronts as (a) the best remote sensing tool available today for global mapping and monitoring of oceanic fronts, and (b) the remote sensing tool providing the longest satellite data set (high-quality SST fields date back to 1982) for retrospective studies.

Oceanic fronts play a major role in marine ecosystems (Le Fevre, 1986; Olson et al., 1994; Longhurst, 2006). The broad importance

* Corresponding author.
E-mail address: igormbelkin@gmail.com (I.M. Belkin).

0079-6611/$ - see front matter © 2009 Elsevier Ltd. All rights reserved.
doi:10.1016/j.pocean.2009.04.015

of fronts stems from their impact on the physical, chemical, and biological environments (Fig. 1). Indeed, density fronts are associated with geostrophic along-front currents that account for the bulk of heat, salt and nutrient transport. These currents also play an important role as conduits for large-scale temperature and salinity anomalies that are well documented in the North Atlantic (e.g. Belkin et al., 1998a; Belkin, 2004), where they profoundly affect regional ecosystems while propagating around the Subarctic Gyre (Greene et al., 2008). These along-front currents maintain and reinforce the division between the different water masses separated by the fronts, thus furthering the relative isolation of the ecosystems associated with these water masses.

Most fronts feature a surface convergence toward the front, at least on one side of the front. Such convergences contribute to elevated primary production at fronts that are known as "hot spots" of marine life, from phytoplankton to apex predators, and are recognized as being spawning, nursing and feeding areas for fish, sea birds, and marine mammals, with high biodiversity. The surface convergence can also lead to concentrations of pollutants, thus endangering frontal species that are attending the fronts.

Fronts can affect both the sea bottom beneath them and the atmosphere above them. The surface convergences at fronts result in downwelling that, combined with elevated primary productivity, can lead to an increase in sedimentation beneath major stable fronts sufficient to leave a geological imprint in sedimentary records. The ocean–atmosphere interaction at major fronts affects not just the relatively thin atmospheric boundary layer but the entire lower part of troposphere (Small et al., 2008; Minobe et al., 2008). The ocean–atmosphere interaction in marginal ice zones results in the formation of oceanic fronts along the sea ice edge in high-latitude seas. In turn, oceanic fronts may limit the extent of sea ice cover, thereby profoundly affecting ecosystems of seasonally ice-covered seas. Finally, oceanic fronts shape the underwater acoustic environment, thus directly impacting whales, dolphins and other species that depend on underwater sound propagation and echolocation for communication, feeding, and migration.

A substantial body of literature exists on the ecology of oceanic fronts, but most studies are focused on individual fronts. At the same time, the concept of Large Marine Ecosystems, LME (Sherman, 1990, 2005) envisions integrated assessments of LMEs, including their hydrography (various maps of LMEs can be found on the official LME Web site, http://www.lme.noaa.gov/). This concept implies a fully-integrated mapping and characterization of the whole frontal pattern in each LME. This can best be achieved through satellite remote sensing thus leading to the major objective of the work presented herein: for each LME, to map all stationary and quasi-stationary SST fronts as proxies for other types of fronts collocated with the SST fronts; to determine their major parameters from satellite and *in situ* data; to quantify their seasonal and long-term variability, and eventually to link fronts and biology, including fisheries, at the scale of individual fronts and individual LMEs. The work in this study is based on a global survey of SST fronts (Belkin et al., 1998b, 2001; Belkin, 2005; Belkin and Cornillon, 2007).

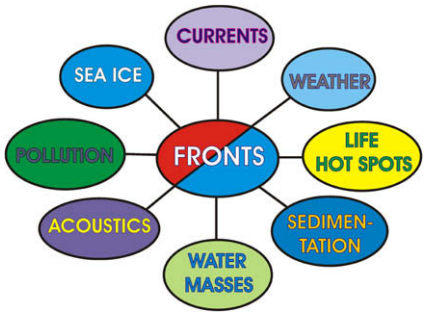

Fig. 1. Impact of oceanic fronts on the oceanic and atmospheric environments (see text for explanation).

This paper is structured as follows. Section 2 describes the front detection algorithm, the satellite data, and the frontal mapping products used in the analysis. Section 3 briefly reviews our main results of the global survey of SST fronts and of the follow-up mapping of SST fronts in the World Ocean LMEs. Section 4 presents frontal patterns in selected regions and draws comparisons between similar frontal zones and ecosystems. Section 5 examines the seasonal evolution of frontal patterns in major upwelling zones. In Section 6 we discuss interdisciplinary cross-cutting issues and present a physically-based classification of LME fronts, thus providing guidelines for comparison studies of frontal ecosystems. Section 7 summarizes the main results. The online Supplementary data contains 64 frontal distribution maps for individual LMEs (Appendix A).

2. Data and methods

The front detection algorithm used in this study is based on histogram analysis. Since a front is a narrow zone between two relatively uniform water masses, a histogram of any oceanographic characteristic (e.g. SST) in the vicinity of the front would have two modes (frequency maxima) corresponding to the two water masses separated by the front, while the front is identified with the frequency minimum between the modes. This idea was implemented by Cayula et al. (1991), Cayula and Cornillon (1992, 1995, 1996) and further developed by Ullman and Cornillon (1999, 2000, 2001). Since the mid-1990s, the Cayula–Cornillon algorithm has been used by various research groups and is considered to be the state-of-the-art front detection tool owing to its robustness and ample worldwide validation (Belkin et al., 1998b, 2001; Ullman and Cornillon, 1999, 2000, 2001; Hickox et al., 2000; Mavor and Bisagni, 2001; Belkin and Cornillon, 2003, 2004, 2005, 2007; Belkin et al., 2003; Nieto and Demarcq, 2006; Miller, 2004, 2009).

Fronts were detected from the NOAA/NASA Pathfinder SST fields (Vazquez et al., 1998) for the period 1985–1996, from 75°N to 75°S. These fields were obtained from the AVHRR (Advanced Very High Resolution Radiometer) Global Area Coverage data stream (two 9.28 km resolution fields per day), available from the Jet Propulsion Laboratory. Each global SST field is a matrix with 2048 rows and 4096 columns. SST fronts were derived from the cloud-masked SST fields with the multi-image edge detection algorithm (Cayula and Cornillon, 1996; Ullman and Cornillon, 1999, 2000, 2001). The cloud masking and front detection algorithms were applied to each of the 8364 SST images in the 12-year sequence.

The multi-image Cayula–Cornillon algorithm consists of three major steps. In the first step, the single image edge detection (SIED) algorithm is applied to each SST field in the time series. The SIED algorithm operates at three levels: image, window, and pixel. The image level portion of the process is associated with the cloud screening algorithm and is not discussed here. At the window level, a histogram analysis is performed on overlapping square windows of pixels in the image. The optimum window size was determined by Cayula and Cornillon (1992) to be 32 by 32 pixels for the global GAC fields as well as for regional 1 km fields. The output of the window level, pixels at the local minimum between two histogram peaks, consists of candidate frontal pixels. The algorithm then descends to the pixel level and follows contours associated with candidate pixels. In the second step of the multi-image process, all frontal segments found in images within approximately 36 hours of each image are merged into a single field and the merged fronts

are thinned. These thinned fronts are then used as candidate frontal pixels for the third step in the multi-image process – a reapplication of the SIED algorithm to all images in the time series.

Three basic types of maps were created and used in the analysis discussed herein: long-term mean frontal frequency maps, quasi-synoptic frontal composite maps, and long-term mean frontal gradient maps. Sample maps of each type are presented in subsequent sections. Long-term mean frontal frequency maps show the pixel-based frequency, F, of fronts normalized by cloudiness: For each pixel, $F = N/C \cdot 100\%$, where N is the number of times during a temporal interval of interest that the given pixel contained a front, and C is the number of times the pixel was cloud-free. Thus, frequency maps are best suited for mapping stable fronts; fronts that move substantially over time result in relatively low frontal frequencies at any given pixel. Long-term mean frontal gradient maps show two scalar quantities, gradient magnitude and gradient direction, associated with each frontal pixel. Frontal gradient magnitude maps give a clear indication of (a) the frontal strength identified with the maximum gradient and (b) the total cross-frontal step of the given property, in this case SST.

The peak of the frontal probability distribution in a given frontal zone or band is determined both by the probability that a front exists in the band and the width of the band – the wider the band, the lower the probability. For fronts associated with widely meandering and shifting currents, the probability can be so small as to almost be lost in the background noise. In such cases quasi-synoptic frontal composite maps are more helpful in locating these fronts because they present all snapshots of fronts detected in individual SST images within a given time period (usually, a week or a month) without any averaging or smoothing. Frontal composite maps are used to detect moving/meandering fronts that are not conspicuous in the frontal frequency maps.

3. Results: global mapping of SST fronts and its application to LME characterization

Long-term mean annual, seasonal, and monthly frontal frequency maps for the Atlantic, Indian, and Pacific Oceans reveal elevated concentrations of quasi-stationary fronts in coastal and marginal seas where all but a few LMEs are located. Based on these maps, the World Ocean was divided into ≈70 overlapping regions for detailed mapping. Long-term mean annual, seasonal, and monthly maps of frontal frequency and gradient were made for these 70 regions that together cover the entire World Ocean between 75°N and 75°S. For each of these 70 regions, 144 monthly (from January 1985 to December 1996) composite frontal maps were made – approximately 10,000 maps in total.

The global frontal data base assembled at URI was used to distinguish patterns of quasi-stationary fronts in the 64 World Ocean LMEs (Belkin, 2005; Belkin and Cornillon, 2007). These frontal patterns are presented here as frontal distribution maps for each LME (Appendix A). Only the most robust, well-defined fronts in each LME are shown regardless of the seasons during which they develop and peak. Therefore each map portrays the long-term annual mean pattern of the fronts. At any given time, only some fronts may be visible in a given LME.

In the next section, frontal patterns in several exemplary LMEs are described in detail. We have chosen these LMEs for their rich frontal patterns and abundant marine life, including major fisheries grounds. As such, these LMEs are highly important economically to adjacent countries. We also show simple analytical tools developed to study spatial and temporal variability of frontal patterns in individual LMEs.

4. Frontal patterns in selected LMEs

4.1. East and West Bering Sea LMEs

4.1.1. East Bering Sea LME

The frontal distribution map for the East Bering Sea LME (Fig. 2) is based on manually digitized frontal paths obtained from 12 long-term monthly frontal frequency maps (Fig. 3, after Belkin and Cornillon, 2005, Fig. 2). Only seven months, from May to November, were used to digitize frontal paths to avoid sea ice cover that is typically present from December to April. Five major fronts were distinguished over the East Bering Shelf and Slope (Belkin and Cornillon, 2005). The Coastal Front consists of three segments, the Bristol Bay Front (BBF), the Kuskokwim Bay Front (KBF), and Shpanberg Strait Front (SSF). These near-coastal fronts likely play an important role in the life of juvenile salmon. Farther offshore, the Inner Shelf Front (ISF) and Mid-Shelf Front (MSF) are approximately isobathic. The most distant offshore fronts, the Outer Shelf Front (OSF) and the Shelf-Slope Front (SSF) are not isobathic. They extend from relatively shallow depths in the east, off Bristol Bay, to significantly greater depths in the west, where the SSF crosses the shelf break and slope to continue over the deep basin as it leaves the East Bering Sea LME and enters the West Bering Sea LME.

4.1.2. West Bering Sea LME

The Shelf-Slope Current bifurcates upstream of Cape Navarin. The northward branch flows toward the Bering Strait as the Anadyr–Chukotka Current associated with the Gulf of Anadyr Front. The southward branch flows first along the Koryak Coast, then along the Kamchatka Peninsula, and is associated, respectively, with the Koryak Coast Current Front and the East Kamchatka Current Front.

4.1.3. Frontal index F1

To characterize temporal variations of spatially-integrated frontal activity within a given area, a very simple frontal index, F1, was introduced by Belkin and Cornillon (2005) and defined as an integral over the entire area of the total number of times each 9-km × 9-km pixel contained an SST front. The resulting index F1 for the entire Bering Sea (Fig. 4, after Belkin and Cornillon 2005, Fig. 10) reveals an extremely strong seasonal variability that dominates interannual variations. Individual annual cycles display a strong year-to-year variability that modulates a unimodal seasonal cycle. Long-term variability is characterized by an ascending trend of F1, which increased approximately 50% from 1985 to 1996. This increase may have profound ecosystem implications, as F1 reflects the total number of SST fronts within the Bering Sea. The above example (see also Belkin and Cornillon, 2005, Figs. 11–13) illustrates the application of this frontal index for integrated assessment of physical and biological conditions in individual LMEs.

4.2. Sea of Okhotsk LME

The frontal schematic of the Sea of Okhotsk LME (Fig. 5) is based on the 12 long-term mean monthly frontal frequency maps published by Belkin and Cornillon (2004). The Okhotsk Sea has a very energetic tidal regime and intense water mass exchange with the open Pacific Ocean. As a result, several different physical types of fronts co-exist there (Belkin and Cornillon, 2003, 2004). A branch of the Kamchatka Current penetrates into the Okhotsk Sea via the First Kuril Strait, to form the West Kamchatka Current Front (WKCF), a water mass front. Robust tidal mixing fronts develop over the western and northern shelves

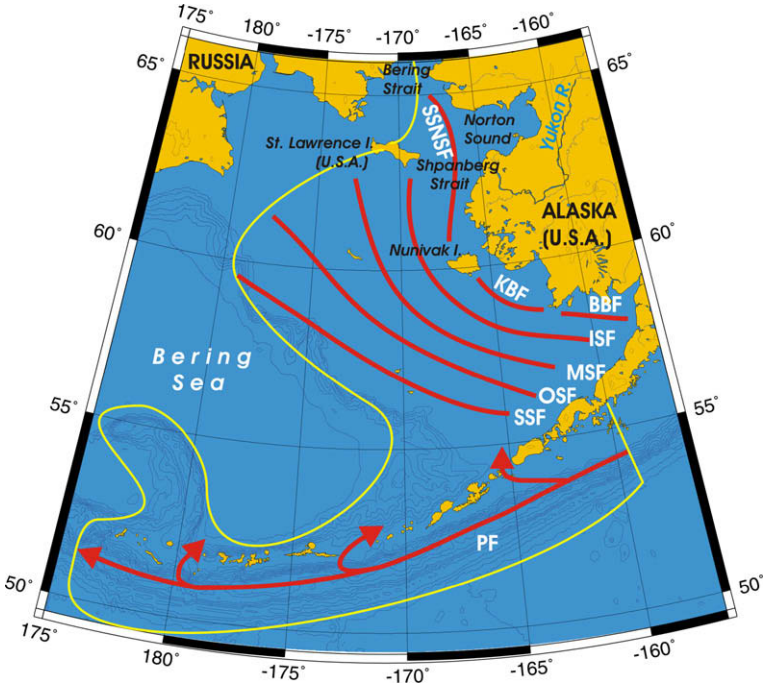

Fig. 2. Fronts of the East Bering Sea LME. Acronyms: BBF, Bristol Bay Front; ISF, Inner Shelf Front; KBF, Kuskokwim Bay Front; MSF, Mid-Shelf Front; OSF, Outer Shelf Front; PF, Polar Front; SSF, Shelf-Slope Front; SSNSF, Shpanberg Strait-Norton Sound Front. Yellow line, LME boundary. After Belkin and Cornillon (2007). This highly generalized schematic summarizes seven long-term monthly frontal patterns for ice-free months (May–November) derived from digitized frontal paths based on 12 years (1985–1996) of satellite SST frontal maps (Belkin and Cornillon, 2005).

(WSF and NSF, respectively), especially off Magadan (MSF) and within Shelikhov Gulf (SGF), where the tidal magnitude peaks at 12–13 m. Very sharp tidal mixing fronts surround Kashevarov Bank (KBF) and the Shantarsky Islands. An estuarine front bounds the Amur River plume; this front continues southward along the east coast of Sakhalin Island as the East Sakhalin Current Front (ESCF).

The Sea of Okhotsk LME is one of the most productive areas of the World Ocean, rivaling the East and West Bering Sea LMEs. It supports fisheries with a total annual catch exceeding 2 million tons, mainly of walleye pollock and also of flounder, herring, and salmon (Belkin and Cornillon, 2004). Our frontal distribution map (Fig. 5) strongly correlates with biomass distributions of phytoplankton, zooplankton, and benthos (Belkin and Cornillon,

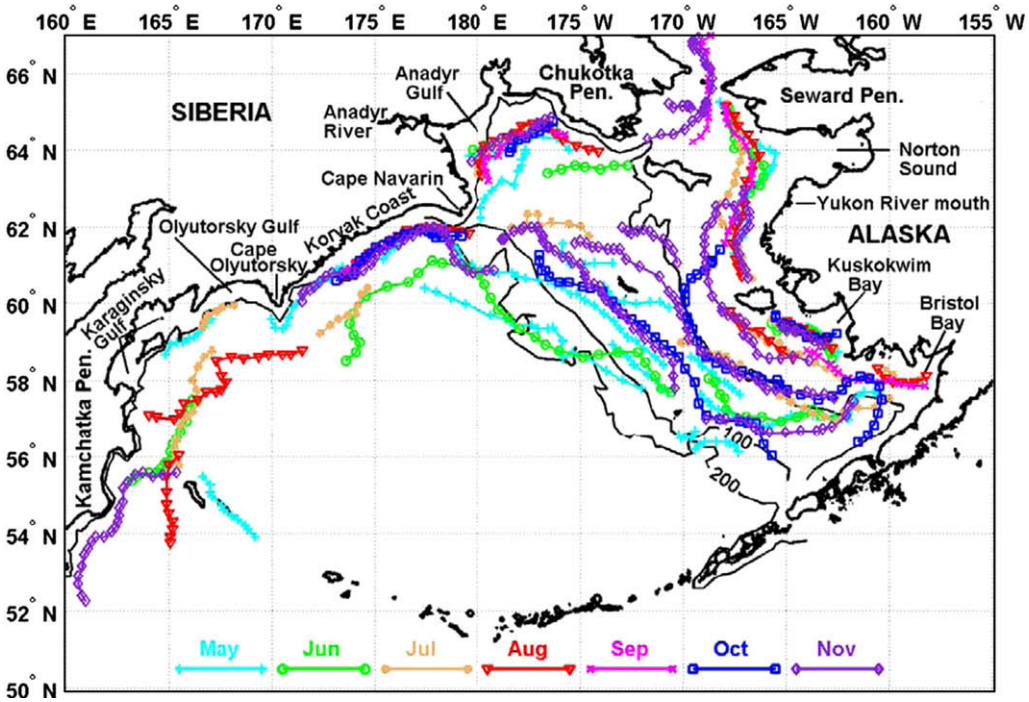

Fig. 3. Seasonal variability of SST fronts in the Bering Sea, May–November 1985–1996 (Belkin and Cornillon, 2005, Fig. 2).

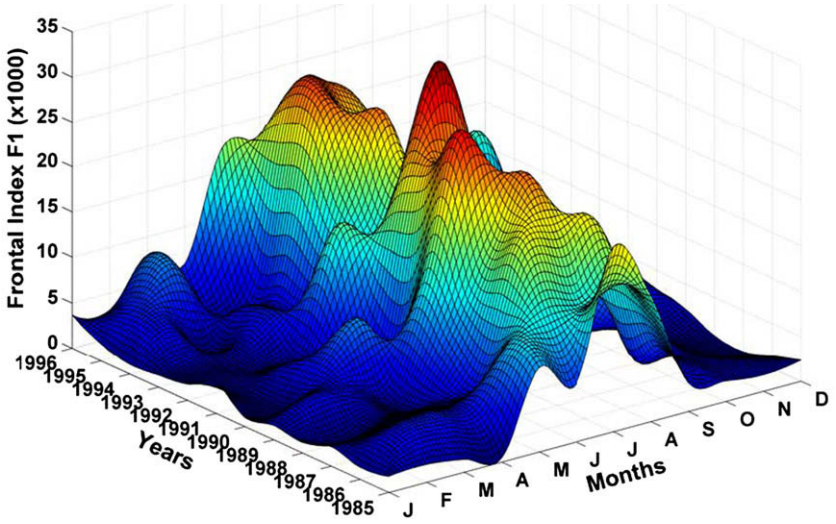

Fig. 4. Temporal variability of the monthly frontal index F1 of the Bering Sea, January 1985–December 1996 (Belkin and Cornillon, 2005, Fig. 10).

2004), and with the faunal zonation of zooplankton (Pinchuk and Paul, 2000, Fig. 2). Pelagic fish and squid tend to concentrate in frontal areas, especially the commercially important walleye pollock. Apex predators such as sea birds and marine mammals also congregate at fronts. The most important breeding ground of northern fur seals in the Sea of Okhotsk LME is located on Robben Island (Ostrov Tyuleniy) off southern end of Sakhalin Island (Gentry, 1998), just a few miles from the East Sakhalin Front that the seals may use as a feeding ground. Steller sea lion rookeries on the Yamsky Islands and on St. Iona Island (NMFS, 1992) are also located close to SST fronts, namely, the North Shelikhov Front and the St. Iona branch of the Kashevarov Bank Front, respectively.

4.3. East China Sea and Yellow Sea LMEs

These LMEs feature extremely stable, primarily wintertime fronts formed by a broad range of physical processes. These fronts have been relatively well studied from satellite data (Hickox et al., 2000; Belkin and Cornillon, 2003) and *in situ* data (Chen, 2009). The types of fronts found in the East China Sea LME (Fig. 6) are more diverse than those found in the Yellow Sea LME. In the northern part of the East China Sea LME, the Yangtze Bank Ring Front (YBRF) surrounds the Yangtze Bank (Shoal). This front is caused by the huge fresh discharge of the Yangtze River (Chang Jiang) and is maintained by tidal rectification that results in a clockwise current and a closed quasi-circular front around the Bank. A water mass

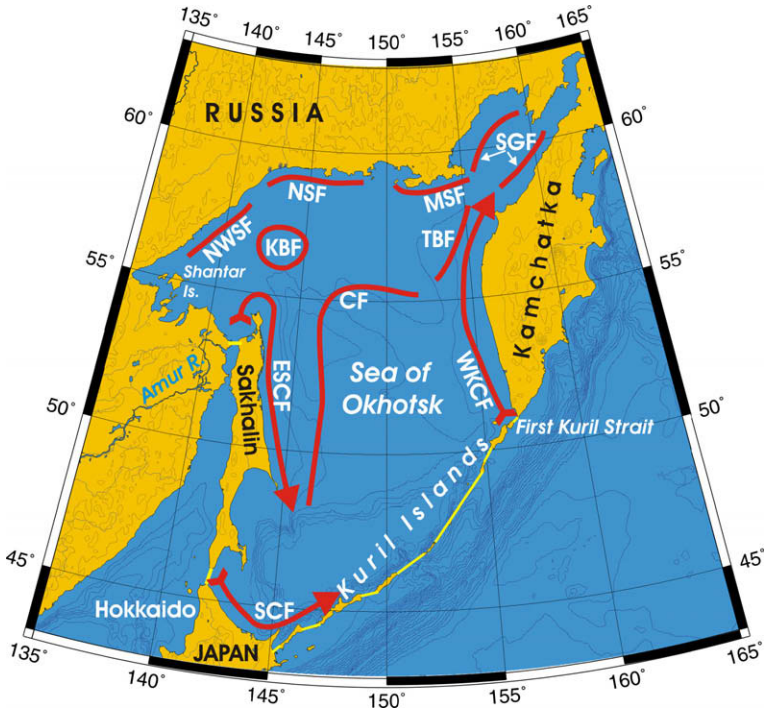

Fig. 5. Fronts of the Sea of Okhotsk LME. Acronyms: CF, Central Front; ESCF, East Sakhalin Current Front; KBF, Kashevarov Bank Front; MSF, Magadan Shelf Front; NSF, North Shelf Front; NWSF, Northwest Shelf Front; SCF, Soya Current Front; SGF, Shelikhov Gulf fronts; TBF, TINRO Basin Front; WKCF, West Kamchatka Current Front. Yellow line, LME boundary. Arrows, along-front currents. After Belkin and Cornillon (2004, Fig. 1).

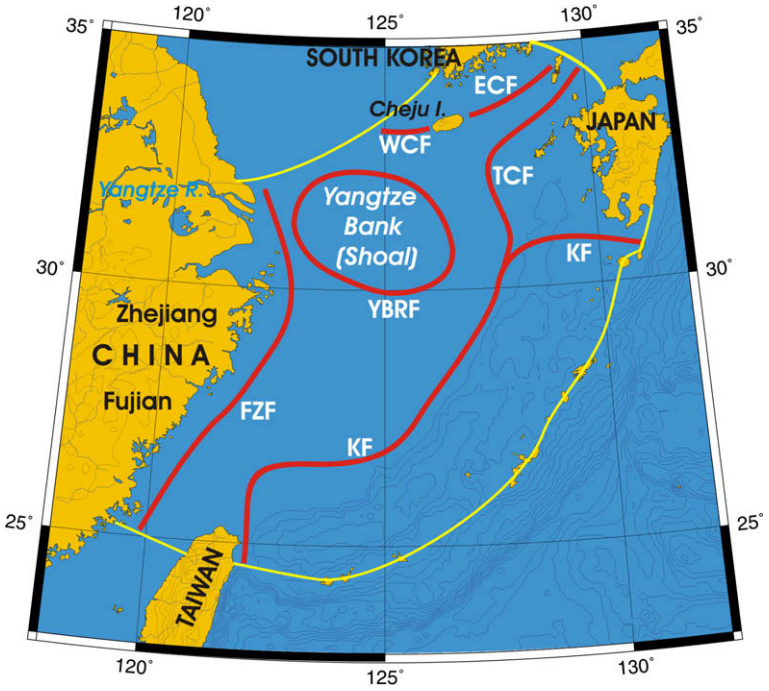

Fig. 6. Fronts of the East China Sea LME. Acronyms: ECF, East Cheju Front; FZF, Fujian–Zhejiang Front; KF, Kuroshio Front; TCF, Tsushima Current Front; WCF, West Cheju Front; YBRF, Yangtze Bank Ring Front. Yellow line, LME boundary. After Belkin and Cornillon (2007), based on Belkin and Cornillon (2003) and Hickox et al. (2000).

front (FZF) runs along the Fujian–Zhejiang Coast between cold, fresh waters flowing southward along the coast and warm, saline offshore waters flowing northward via the Taiwan Strait. The Kuroshio Front (KF) invades the shelf north of Taiwan. These excursions are important for the cross-shelf exchange of heat, salt and nutrients. Sharp fronts (WCF and ECF) separate the warm, saline waters of the Kuroshio Current and the colder, fresher coastal waters off Cheju Island. In the Yellow Sea LME, the most robust fronts are tidal mixing fronts around the Shandong Peninsula, off Jiangsu Shoal, and off the West Korea and Kyonggi bays (Hickox et al., 2000; Belkin and Cornillon, 2003). The freshwater discharge of the Yellow River (Huang He) plays a minor role in maintaining Yellow Sea fronts compared with the role of the Yangtze River in maintaining East China Sea fronts.

Satellite data reveal a variety of annual cycles of SST fronts in both LMEs (Fig. 7) depending on the frontal structure and the physical mechanisms responsible for the front formation, e.g. tidal mixing, water mass convergence, river runoff, and deep winter convection. Some fronts reverse seasonally, as their cross-frontal gradient changes its sign from winter to summer (Fig. 7). For example, the Yangtze River plume surrounded by the Yangtze Bank Ring Front (YRBF) is warmer than the ocean waters in spring–summer, but colder during the rest of the year.

4.4. North Sea LME

The North Sea LME is rich with diverse fronts (Fig. 8). Most fronts are best defined in winter. Tidal mixing, river runoff, and upwelling fronts dominate the sea (Krause et al., 1986; Otto et al., 1990). The Kattegat–Skagerrak Front is a water mass front (Omstedt et al., 2004; Nielsen, 2005). Near the Norwegian coast, salinity fronts caused by the fresh runoff from fjords and the low

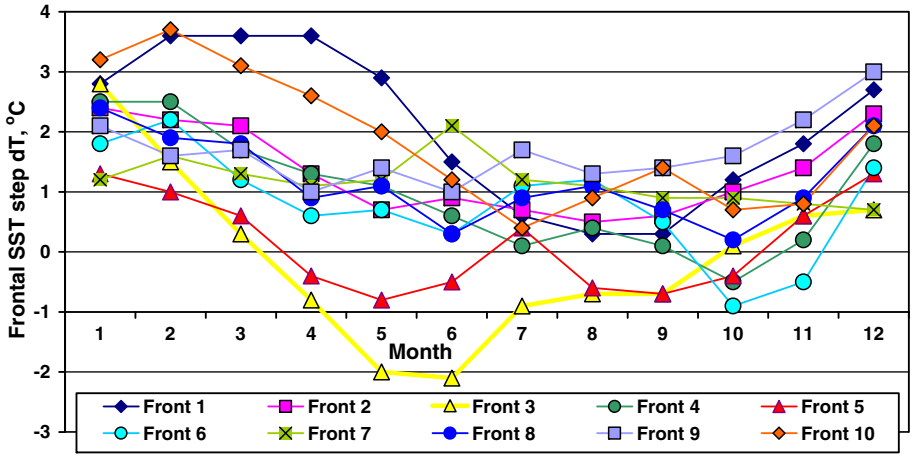

Fig. 7. Seasonal variability of SST ranges across fronts of the Yellow and East China Sea LMEs. The cross-frontal SST range $dT = SST_{offshore} - SST_{inshore}$. Based on the results obtained by Hickox et al. (2000).

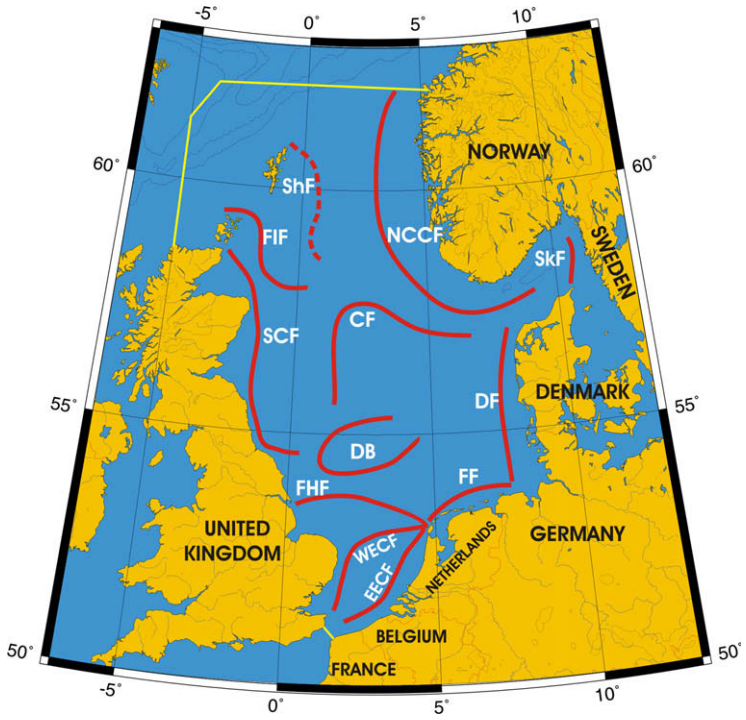

Fig. 8. Fronts of the North Sea LME. Acronyms: CF, Central Front; DBF, Dogger Bank Front; EECF, East English Channel Front; FF, Frisian Front; FHF, Flamborough Head Front; FIF, Fair Isle Front; NCCF, Norwegian Coastal Current Front; ShF, Shetland Front; SkF, Skagerrak Front; WECF, West English Channel Front. Yellow line, LME boundary. After Belkin and Cornillon (2007).

salinity Skagerrak outflow are observed at all times, sometimes associated with temperature fronts. Salinity fronts are also ubiquitous in the southern North Sea, where they are caused primarily by the outflows of the Rhine, Scheldt, and Elbe rivers. We observe a number of SST fronts apparently associated with these salinity fronts, aligned in the meridional direction, similar to the fronts shown by Otto et al. (1990). The Fair Isle Current Front (FICF) was known to be pronounced in summer and has been considered absent in winter (Otto et al., 1990). We detected the FICF year-round and the best example of the FICF comes from the wintertime satellite imagery.

4.5. East and West Greenland Shelf LMEs and Newfoundland–Labrador Shelf LME

The three LMEs that surround the Atlantic Subarctic Gyre are connected by similar fronts and have analogous frontal patterns that feature (a) strong and robust shelf-slope fronts that separate oceanic and shelf water masses, and (b) mid-shelf/inner-shelf fronts that separate shelf water masses from near-shore/coastal water masses strongly affected by freshwater runoff.

4.5.1. East Greenland Shelf LME

The Polar Front associated with the East Greenland Current, the East Greenland Polar Front (EGPF), extends along the shelf break east of Greenland (Fig. 9). Though the EGPF location is generally closely associated with the continental slope, a noteworthy exception is observed at 64–65°N, 40–35°W, where the EGPF splits. The offshore branch continues along the shelf break, whereas the inshore branch extends well onto the broad shelf off Ammassalik and rejoins the offshore branch farther downstream. This double front, tentatively named the Ammassalik Front, is a newly found feature. The newly found multi-frontal pattern over the Ammassalik Shelf may have important ramifications in fisheries oceanography since this shelf is a major spawning ground of cod.

4.5.2. West Greenland Shelf LME

The West Greenland shelf break steers the West Greenland Current and the associated front until ~63°N, 53°W. As the West Greenland continental slope becomes less steep and the shelf break more poorly defined, it fails to steer the West Greenland Current Front (Fig. 9). At this point the current becomes prone to vigorous meandering and eddy formation; the front is no longer well defined in this map. Another frontal discontinuity is observed off the entrance to Hudson Strait, where the southward flowing Baffin Current meets the fresh Hudson Strait outflow.

4.5.3. Newfoundland–Labrador Shelf LME

South of Hudson Strait, two fronts are visible: the offshore front associated with the main branch of the Labrador Current and the mid-shelf front associated with the Hudson Strait outflow. The offshore front is a well-known feature, whereas the mid-shelf front has not been described in the literature. The mid-shelf Labrador Front apparently plays an important role in the life of Greenland halibut as evidenced by regular Canadian halibut surveys.

4.6. Gulf of Mexico LME; Southeast and Northeast US Continental Shelf LMEs

The large-scale frontal patterns in the Gulf of Mexico LME, Southeast US Continental Shelf LME (especially, in the South Atlantic Bight, SAB) and Northeast US Continental Shelf LME (especially, in the Mid-Atlantic Bight, MAB) are seasonally persistent (Figs. 10–12) as most fronts are steered by bottom topography, particularly by the well-defined shelf break and the steep upper continental slope.

4.6.1. Gulf of Mexico LME

Thermal fronts in the Gulf of Mexico (Fig. 11) display a strong seasonal signal; in summer few fronts are visible in SST imagery because seasonal warming obliterates the surface signatures of

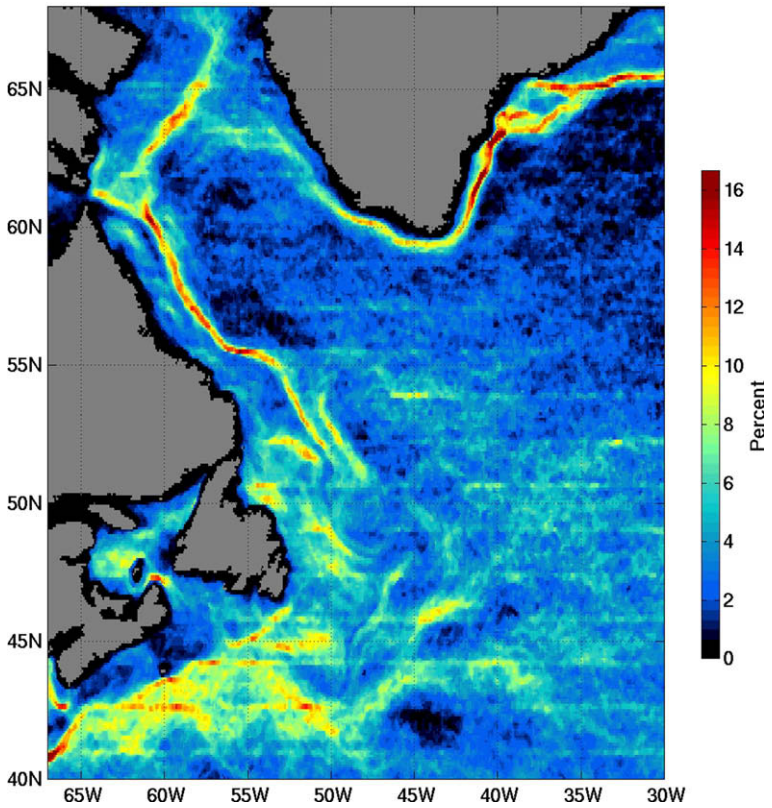

Fig. 9. Long-term mean summer frequency of SST fronts in the Northwest Atlantic, July–September 1985–1996.

most fronts. The Campeche Bank Front (a mid-shelf front along 22°N) is an exception, since it persists in June–August when this front is the only distinct feature in the SST field in the Gulf. Other fronts emerge in October–November, especially the shelf break fronts and the mid-shelf fronts, in the northern Gulf and the western Gulf. The mid-shelf fronts form in the Gulf due to cold air outbreaks (Huh et al., 1978). Fronts proliferate in winter when a robust pattern of several prominent fronts emerges, which are associated with the Yucatan Current, Loop Current, warm-core anticyclonic rings of the Loop Current, shelf break fronts, and mid-shelf fronts over the West Florida, Texas–Louisiana, and western Campeche Bank shelves.

An intense flow from the Caribbean Sea into the Gulf of Mexico, known as the Yucatan Current, is associated with a very strong and persistent frontal zone on its western side that separates the current's unproductive water from the biologically very rich waters of the Campeche Bank (Perez et al., 1999). The front is evident year round, even in summer when the horizontal SST gradients are weak. The persistence of this front is accounted for by the coastal upwelling that is strong enough to maintain a substantial horizon-

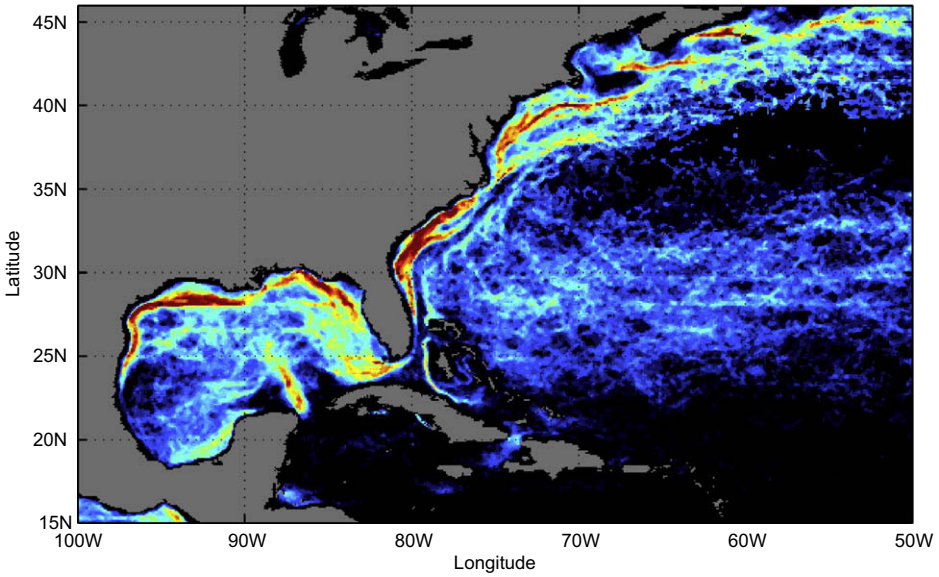

Fig. 10. Long-term mean (1985–1996) March frequency of SST fronts in the Western North Atlantic.

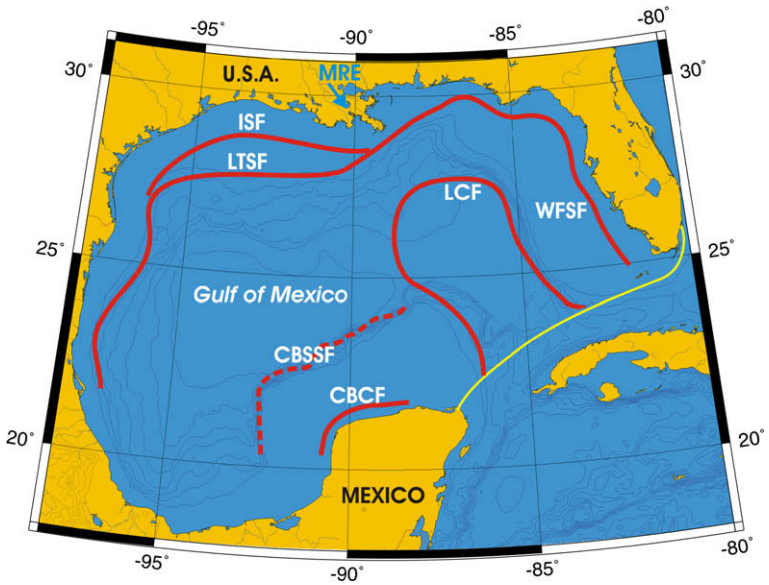

Fig. 11. Fronts of the Gulf of Mexico LME. Acronyms: CBCF, Campeche Bank Coastal Front; CBSSF, Campeche Bank Shelf-Slope Front (most probable location); ISF, Inner Shelf Front; LCF, Loop Current Front; LTSF, Louisiana–Texas Shelf Front; MRE, Mississippi River Estuary; WFSF, West Florida Shelf Front. Yellow line, LME boundary. After Belkin and Cornillon (2007).

tal SST gradient off northern Yucatan (Perez et al., 1999). This upwelling is an example of a western boundary upwelling as opposed to the well-known, extensive eastern boundary wind-driven upwellings. The exact mechanism of the Yucatan upwelling is unknown; it is probably caused by bottom friction or other topographic mechanisms (Merino, 1997).

4.6.2. Southeast US Continental Shelf LME

In the surface layer, the Florida Current and the Gulf Stream are bordered by two fronts that correspond to their cold and warm sides. Both fronts can be seen year-round in the seasonal frequency maps (Fig. 10). The cold-side front (sometimes referred to as the "cold wall" or the "north wall" of the Gulf Stream) is better defined compared to the warm-side front. The SST step across the cold front ranges from 2 °C in August up to 10 °C in March. The warm-side front, albeit less strong than the cold front, is systematically detected in satellite SST imagery, with the cross-frontal SST range varying seasonally from 1.5 °C to 4.5 °C. A quasi-stationary deflection of the Gulf Stream downstream of the Charleston Bump is evident at 32°N. This frontal feature is associated with the

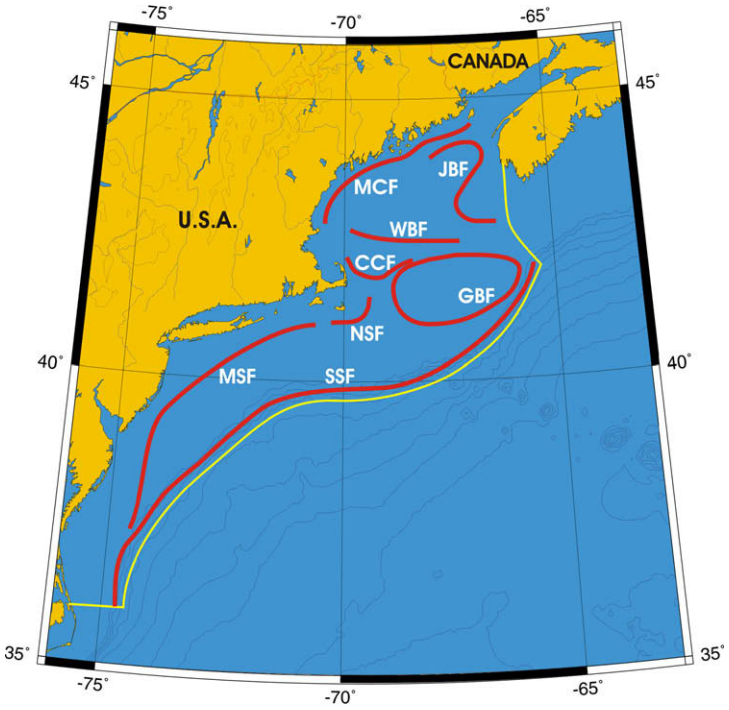

Fig. 12. Fronts of the Northeast US Continental Shelf LME. Acronyms: CCF, Cape Cod Front; GBF, Georges Bank Front; JBF, Jordan Basin Front; MCF, Maine Coastal Front; MSF, Mid-Shelf Front; NSF, Nantucket Shoals Front; SSF, Shelf-Slope Front; WBF, Wilkinson Basin Front. Yellow line, LME boundary. After Belkin and Cornillon (2007).

Charleston Bump, an important fish habitat in the Gulf Stream (Sedberry et al., 2001). Farther downstream of the Bump, the quasi-stationary cyclonic Charleston Gyre forms, an important spawning and larval fish habitat (Govoni and Hare, 2001).

Located west of the Gulf Stream in the SAB is the Mid-Shelf Front (MSF) (Fig. 10). This front is more stable than the Gulf Stream fronts; therefore it appears more prominently than the Gulf Stream. The separation between these fronts is maximal near the SAB apex (31°N), apparently because of the northward isobath divergence; and downstream of the Charleston Bump (east of 79°W), owing to the Gulf Stream veering east (Fig. 10).

The SAB MSF is different from the MAB MSF described by Ullman and Cornillon (1999) in that: (a) unlike its northern counterpart, which is only detected in winter, the SAB MSF is distinct in fall, winter, and spring, and; (b) the SAB MSF extends over shallower depths (20–40 m) whereas the MAB Mid-Shelf Front is centered around the 50 m isobath. The MSF is important to the SAB ecology, attracting fish and sea birds; the latter's spatial density near this front is an order of magnitude above the background (Haney and McGillivary, 1985).

4.6.3. Northeast US Continental Shelf LME

The most persistent feature of this LME is the Shelf-Slope Front that extends south of New England (Figs. 10 and 12) and is well known as an important fishing ground. The modal (most likely) path of this front closely follows the shelf break. In winter, the Mid-Shelf Front is seen inshore of the Shelf-Slope Front, centered over the 50 m isobath (Ullman and Cornillon, 1999). The Mid-Shelf Front has different characteristics in the Northeast and Southeast US Continental Shelf LMEs with respect to water depth, seasonal variability, and forcing. In summer and early fall, tidal mixing fronts emerge north of Nantucket Shoals, in the Gulf of Maine, and around Georges Bank (Ullman and Cornillon, 1999; Mavor and Bisagni, 2001).

4.7. Patagonian Shelf LME

The Patagonian Shelf LME occupies the largest continental shelf of the Southern Ocean and one of the largest shelves in the World Ocean. This shelf features extremely rich frontal patterns in all seasons (Fig. 13). Three year-round fronts are evident on the Patagonian Shelf:

(1) Valdés Front, VF, after Península Valdés at 42°S.
(2) San Jorge Front, SJF, after Golfo San Jorge at 46°S.
(3) Bahia Grande Front, BGF, after a bay at 51°S.

The origin of the VF and the SJF is likely related to regions of enhanced tidal mixing located near Península Valdés and near both ends of Golfo San Matías where tidal fronts are formed separating well-mixed water from stratified water in spring and summer (Glorioso and Flather, 1997). Two seasonally persistent fronts are distinguished over the Patagonian Shelf, namely the Bahia Blanca Front, BBF (after a bay at 39°S), and the Magellan Front, MF, located near the eastern entrance to the Strait of Magellan. In fall (April–June), this front consists of two distinct branches, northern and southern, termed the Patagonian–Magellan Front, PMF, and Tierra del Fuego Front, TFF, respectively. The origin of MF, PMF, and TFF is likely related to the influx of relatively cold, fresh water from the SE Pacific via the Strait of Magellan and also probably around the southern tip of Tierra del Fuego (with the Cape Horn Current). The Patagonian shelf break front has an unusual structure with multiple fronts parallel to the shelf break (Franco et al., 2008). The biological significance of the Patagonian fronts was highlighted by Acha et al. (2004) and Rivas (2006).

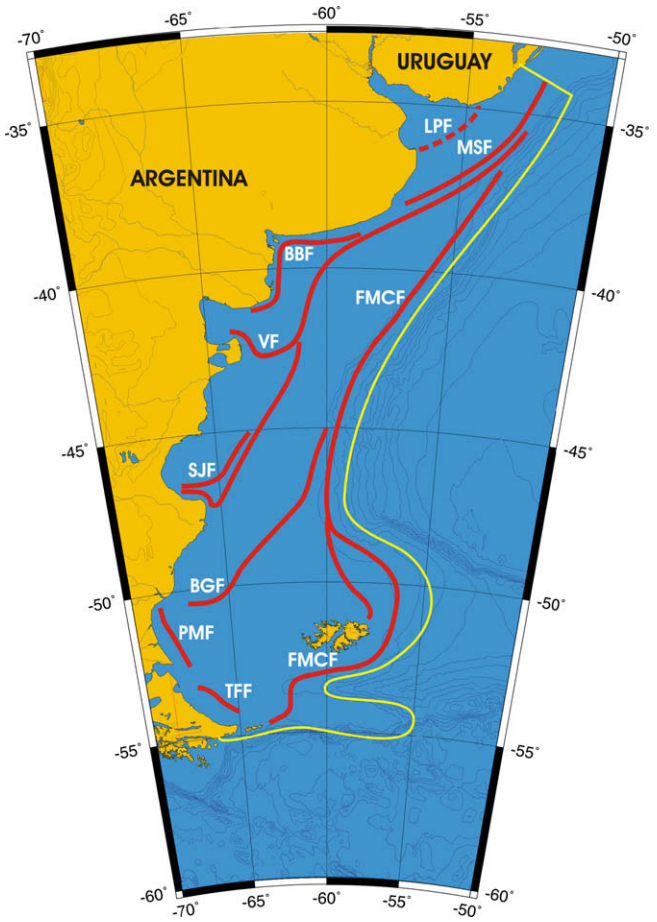

Fig. 13. Fronts of the Patagonian Shelf LME. Acronyms: BBF, Bahia Blanca Front; BGF, Bahia Grande Front; FMCF, Falkland/Malvinas Current Front; LPF, La Plata Front; MSF, Mid-Shelf Front; PMF, Patagonian–Magellan Front; SJF, San Jorge Front; TFF, Tierra del Fuego Front; VF, Valdes Front. Yellow line, the LME boundary. After Belkin and Cornillon (2007).

5. Seasonal evolution of frontal pattern in major upwelling LMEs

Frontal frequency maps emphasize stationary and quasi-stationary fronts that owe their stability to the bathymetry that steers them. Such maps tend to understate dynamic fronts associated with meandering and lateral shifts, or transient fronts that emerge and dissipate over relatively short time scales, 1–10 days. Such fronts are best studied with the help of quasi-synoptic frontal composite maps that display all instantaneous fronts detected in individual satellite images and aggregated over a period of time that is an order of magnitude shorter than the time scale of interest. Since our main focus at this point is on the annual cycle of frontal patterns in individual LMEs, monthly frontal composites (aggregates) serve this purpose.

Fig. 14 presents two monthly composite frontal SST maps for the California Current LME. Even a cursory comparison of these two maps makes obvious a dramatic change of the entire frontal pattern from an apparent chaotic pattern of small-scale fronts in summer to a quasi-regular pattern of several huge filaments, up to 1000 km long, extending northwest from the Oregon–California–Baja California coast, spaced a few hundred km apart in winter. Each of these filaments was coherent for at least the duration of the composite mapping period, one month. This drastic seasonal change of the entire frontal pattern has not been reported before

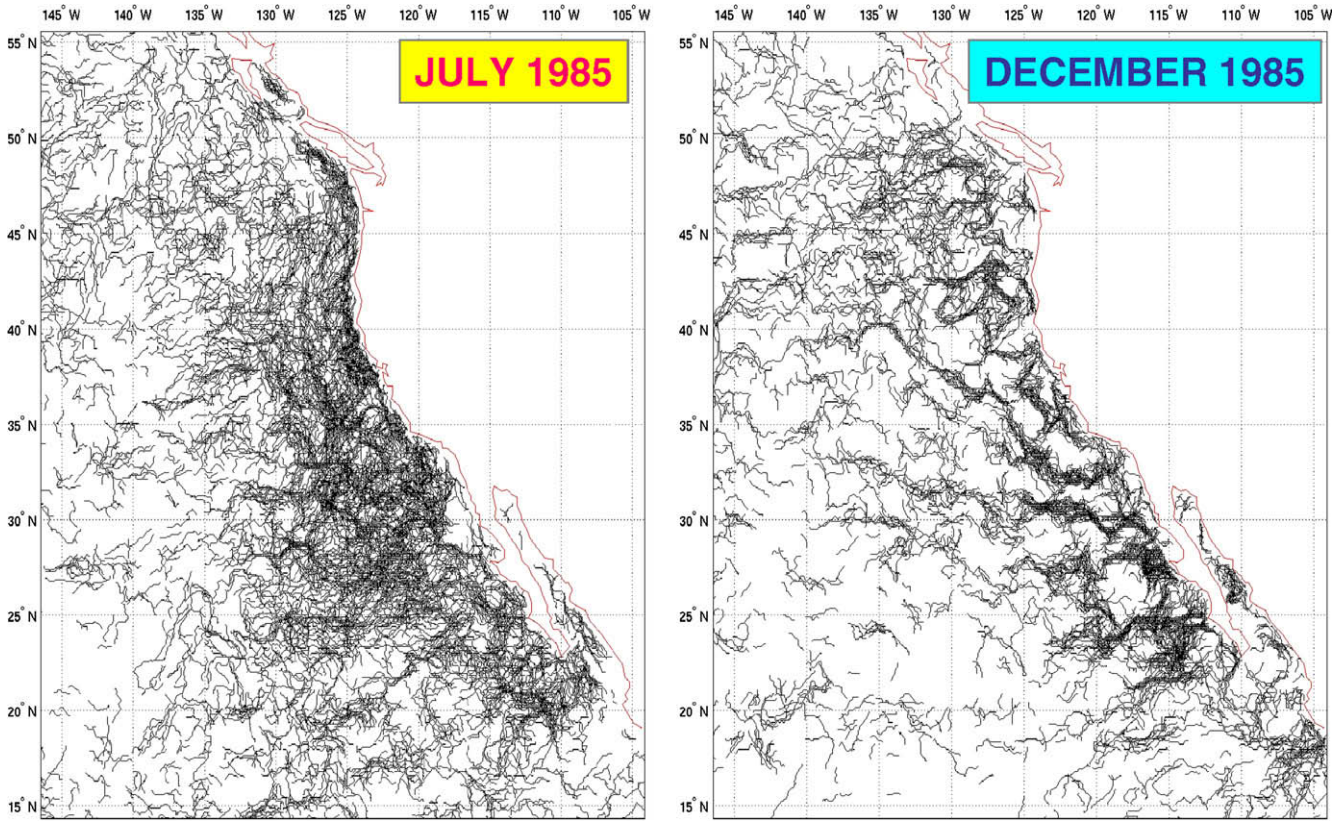

Fig. 14. Seasonal evolution of SST frontal pattern in the California Current LME. Shown are monthly frontal composite maps from July 1985 (left) and December 1985 (right).

(cf. Hickey, 1998). What makes this phenomenon all the more important globally is that a similar evolution of regional frontal patterns is observed from our data in other eastern boundary upwelling LMEs, notably in the Canary Current LME, in the Arabian Sea LME, in the Northwest Australian Shelf LME, in the northern part of the Humboldt Current LME (Peruvian upwelling), and in the Benguela Current LME.

The above-noted seasonal evolution of frontal patterns in major upwelling LMEs can be expressed in terms of the dominant spatial scale of individual fronts. In the California Current LME, this scale increases by an order of magnitude from summer to winter (Fig. 14). From a visual inspection of monthly composites, from January 1985 to December 1996, in all six major eastern boundary upwelling LMEs noted above, the dominant frontal scale increases at least 10-fold from summer to winter. The California Current LME is the only area where these filaments form a quasi-regular unidirectional pattern, with the large-scale coherent filaments in winter extending 500–1000 km offshore, trending ESE–WNW (Fig. 14, right). In other upwelling LMEs, such large-scale coherent wintertime fronts do not exhibit a dominant spatial orientation, so the entire frontal pattern is approximately isotropic. The anisotropy of the California upwelling frontal pattern in winter is likely linked to the seasonal evolution of the large-scale wind stress field.

The biological significance of such large-scale filaments stems from the observations that these filaments carry the bulk of the cross-shelf/slope transport of nutrients (Lutjeharms et al., 1991). The jet-like along-front currents associated with these filaments could transport larvae and juvenile fish hundreds of kilometers offshore, contributing to their dispersal (Lutjeharms et al., 1991). The spatial and temporal scales of these features inferred from synoptic satellite frontal maps provide observational constraints on models of larval dispersal.

6. Discussion: frontal classification and comparison of LMEs

Analysis of 12 years of satellite SST data reveals rich frontal patterns in most LMEs, which are presented in previous sections and Appendix A. Many of these fronts have never been described in the literature, and most of them have not been a subject of a dedicated field or remote sensing study. The paucity of front-resolving *in situ* data is the main reason why our knowledge of the physical mechanisms that create and maintain these fronts is rudimentary at best. And yet, it is the physics of fronts that holds clues to understanding frontogenesis and frontolysis and eventually to front modeling and forecasting, including modeling of physical–biological interactions at fronts. Therefore we propose a provisional classification of LMEs based on their frontal pattern (Table 1). The suggested classification includes only those fronts whose nature is reasonably well established and is based on the entire body of the literature on the oceanography of fronts and frontal zones readily available in English, as well as selected articles in other languages. A small part of this bibliography is cited by Belkin and Cornillon (2007). Regional bibliographies of the North Pacific and Arctic LMEs can be found in Belkin and Cornillon (2003, 2004, 2005), Belkin et al. (2003), and Hickox et al. (2000).

Different ecosystems are populated by different types of fronts depending on dominant physical processes in these ecosystems. Most important mechanisms are tides, upwelling, water mass convergence, and fresh water inflows. Since tides are ubiquitous, so are tidal mixing fronts (TMF), although the strength and persistence of TMFs depend on tidal characteristics. The exact locations of TMFs also depend on bathymetry. Some TMFs are locked into topographic steps such as submarine terraces or submerged shores. The suggested classification emphasizes those fronts that dominate in a given LME. Most LMEs include fronts of various types.

Table 1
Frontal classification of large marine ecosystems.

Type T: LMEs with tidal mixing fronts. Examples: East Bering Sea LME; Sea of Okhotsk LME; Gulf of Alaska LME; North Sea LME; Yellow and East China Sea LMEs; Patagonian Shelf LME; Faroe Plateau LME.
Type F: LMEs with freshwater inflows. Examples: East and West Bering Sea LMEs; Sea of Okhotsk LME; Yellow and East China Sea LMEs; Patagonian Shelf LME; Gulf of Alaska LME; Baltic, North, and Norwegian Sea LMEs; East and West Greenland Shelf LMEs; Newfoundland–Labrador and Scotian Shelf LMEs; Bay of Bengal LME; Gulf of Thailand LME; North Australian Shelf LME.
Type U: LMEs with upwelling fronts. Wind-driven coastal, wind-driven equatorial, and topographic (bathymetric) upwellings. Examples: California Current LME, Humboldt Current LME; Canary Current LME; Benguela Current LME; Arabian Sea LME; Northwest Australian Shelf LME.
Type W: LMEs with western boundary current fronts. Examples: Northeast and Southwest US Continental Shelf LMEs; Gulf of Mexico LME; East and West Greenland Shelf LMEs; Newfoundland–Labrador Shelf LME; Somali Coastal Current LME; Agulhas Current LME; East-Central Australian Shelf LME; Kuroshio and Oyashio Current LMEs.
Type E: LMEs with eastern boundary current fronts. Examples: West-Central Australian Shelf LME; California and Humboldt Current LMEs; Canary and Benguela Current LMEs.
Type C: LMEs with water mass convergence fronts. Examples: Northeast US Continental Shelf LME; Patagonian Shelf LME; Iceland Shelf LME

Table 2
LMEs dominated by tidal mixing fronts.

LME	Front types	Net SST Change 1982–2006 (°C)
North Sea	T, F, C, E	1.31
East China Sea	T, R, W, C	1.22
Yellow Sea	T, R	0.67
Sea of Okhotsk	T, R, C	0.31
NE US Continental Shelf	T, F, C, W	0.23
Patagonian Shelf	T, W	0.08

Table 4
LMEs dominated by western boundary currents and shelf-slope fronts.

LME	Front types	Net SST Change 1982–2006 (°C)
East Greenland Shelf	W, C, F	0.47
West Greenland Shelf	W, C, F	0.73
Newfoundland–Labrador Shelf	W, C, F	1.04
Scotian Shelf	W, C, F, T	0.89
NE US Continental Shelf	W, C, F, T	0.23

The front-based classification of LMEs can serve as a framework for comparison studies of LMEs. We assembled four prospective comparison studies in Tables 2–5 that contain information on dominant frontal types (from the above classification) and estimates of the net SST change in 1982–2006 in each LME (Belkin, 2009). Primary productivity data for these LMEs is available from Sherman et al. (2009). A brief summary of the comparison studies is provided below.

LMEs dominated by tidal mixing fronts (Table 2). A comparison study of the North Sea LME vs. East China and Yellow Sea LMEs is warranted, as both areas are dominated by tidal mixing fronts and also both areas experienced a rapid warming in 1982–2006 (Belkin, 2009). Another comparison study is warranted between the Sea of Okhotsk LME and the Northeast US Continental Shelf LME since these LMEs feature similar large embayments (Shelikhov Bay and Penzhina Bay in the northeastern Okhotsk Sea and Bay of Fundy in the Gulf of Maine) with the world's largest tides and robust tidal mixing fronts.

LMEs dominated by upwelling fronts (Table 3). Both upwelling LMEs in the Eastern Pacific (California and Humboldt) cooled while other four major upwelling LMEs warmed. The cooling is consistent with the Bakun (1990) upwelling intensification mechanism, whereas the warming is not. A comparison study between the California and Humboldt Current LMEs is warranted as well as a comparison study of the two cooling LMEs versus the four warming LMEs.

LMEs dominated by western boundary currents and shelf-slope fronts (Table 4). In the Northwest Atlantic, five LMEs along North America's eastern seaboard need to be analyzed in the advective framework since they are connected by shelf-slope currents that transport anomalies of physical, chemical and biological properties from one LME to another.

LMEs with strong estuarine and river plume fronts (Table 5). River runoff may exacerbate regional manifestations of global warming (Belkin, 2009). The East China Sea LME and Black Sea LME include major shelf fronts that are maintained by river discharge; both seas experienced a super-fast warming. A comparison study is warranted of those LMEs from Table 5 that have similar frontal patterns and other parameters, e.g. river runoff, warming rate, etc.

6.1. Seasonal evolution of fronts

In most high-latitude LMEs, SST fronts emerge in late spring and summer and disappear in winter. The set-up of summer stratification on the offshore side of tidal mixing fronts (TMF) enhances cross-front gradients, thus strengthening the TMFs through the warming season. Spring freshets create strong salinity fronts that are often accompanied by temperature fronts. For example, in the California Current LME, the Columbia River outflow in spring is much colder than the coastal ocean and is clearly visible in satellite SST images. In late spring and summer, most river plumes are warmer than the coastal waters, e.g. the Danube River plume in the Black Sea LME or the Yangtze River plume in the East China Sea LME. Salinity fronts associated with river runoff are often accompanied by thermal fronts as the buoyant freshwater plume traps solar heat during the warming season, thereby enhancing the temperature contrast across the plume front. Examples of such development are observed in the Patagonian Shelf LME (Rio de la Plata

Table 3
LMEs dominated by upwelling fronts.

LME	Front types	Net SST Change 1982–2006 (°C)
California Current	U, E, C	−0.07
Humboldt Current	U, E	−0.10
Canary Current	U, E	0.52
Benguela Current	U, E	0.24
Arabian Sea	U, C	0.26
NW Australian Shelf	U, T, E	0.24

Table 5
LMEs with strong estuarine and river plume fronts.

LME	Front types	Net SST Change 1982–2006 (°C)
East China Sea	F, T, C, W	1.22
North Sea	F, T	1.31
Black Sea	F, C	0.96
Patagonian Shelf	F, T	0.08
Gulf of Mexico	F, C, W, T	0.31
Bay of Bengal	F	0.24
Gulf of Thailand	F	0.16
Sea of Okhotsk	F, T, C, W	0.31
North Brazil Shelf	F	0.60
Guinea Current	F	0.46

plume) and in the Scotian Shelf LME, where the St. Lawrence River outflow mostly affects the Scotian Shelf LME but also may affect the Newfoundland–Labrador Shelf LME.

6.2. Topographic control of oceanic fronts

The great majority of stable fronts are steered by ocean bottom topography. The shelf break and upper continental slope play the most important role in stabilizing their respective fronts. A convoluted shelf break and/or large canyons tend to disrupt and destabilize the shelf-slope front. For example, in the East Bering Sea LME, the extremely rugged continental slope incised by the world's largest canyons does not exert strong control on the Slope Current and the associated Shelf-Slope Front (Belkin and Cornillon, 2005) that meander widely and spawn eddies and rings that greatly enhance the cross-frontal transport of nutrients. The elevated productivity of the "Green Belt" in the East Bering Sea LME results likely from this vigorous eddy variability caused by the Slope Current interaction with the canyon-incised slope. A similar situation exists in the West Greenland Shelf LME, where the northward flowing West Greenland Current becomes destabilized by complex topography west of 53°W (Section 4.5), while remaining stable upstream, where the continental slope is steep and the shelf break is well defined. Parallels also might be drawn between the East Bering Sea Slope and the western slope of the Iberian Peninsula (Iberian Coastal LME), where the northward coastal current encounters extremely steep canyons and capes, resulting in the formation of large subsurface lenses of Mediterranean water ("Meddies"). In contrast, the northward flowing West Kamchatka Current in the Sea of Okhotsk LME does not experience major disruptions thanks to the relatively smooth continental slope.

6.3. Oceanic fronts as hot spots of marine life

The frontal frequency maps analyzed in this study contain a wealth of information about biological "hot spots" that correspond to local maxima of frontal frequency. Some of these "hot spots" are well-known, e.g. the Cape Bathurst polynya in the Beaufort Sea LME where highest concentrations of marine mammals and sea birds are observed exactly where the continental slope is the steepest and, as a result, the shelf-slope front is most stable (Belkin et al., 2003). Another example is Melville Bay in the upper Baffin Bay (West Greenland Shelf LME), the famous whaling ground that has been known since the mid-19th century. A newly-found front over a major bank may be important to the local populations of seals and beluga whales that migrate across this area. Other potential "hot spots" detected in frontal frequency maps have not been studied yet, e.g. the frontal "hot spots" in the East Bering Sea LME (Belkin and Cornillon, 2005).

7. Summary

Oceanic frontal patterns and individual fronts are recognized as important physical factors shaping marine ecosystems. This realization stimulated a renewed interest in frontal mapping and characterization. The first global remote sensing survey of thermal fronts has led to provisional mapping of the fronts in the World Ocean Large Marine Ecosystems (LMEs) presented in this paper. The front detection and cloud-masking algorithms (Cayula and Cornillon, 1992, 1995, 1996) were run on 12 years (1985–1996) of Pathfinder 9 km resolution twice-daily AVHRR SST fields, to map fronts in each synoptic (nearly instantaneous) image and eventually compute long-term frequencies of SST fronts and their gradients. These maps were analyzed to distinguish major stationary, robust fronts and derive provisional frontal schematics for all LMEs that can be used to guide field studies of marine ecosystems and place biological findings, especially spatial distributions, into a frontal reference frame. The SST fronts found here can be used as pointers to fronts in other properties, e.g. salinity, density, nutrients, and chlorophyll, known to be collocated with the SST fronts described. The fronts of selected LMEs are described in detail and compared, including the East and West Bering Sea LMEs; the Sea of Okhotsk LME; the East China Sea and Yellow Sea LMEs; the North Sea LME; the East and West Greenland Shelf LMEs; the Newfoundland–Labrador Shelf LME; the Gulf of Mexico LME; the Southeast and Northeast US Continental Shelf LMEs; and the Patagonian Shelf LME. In major eastern boundary upwelling LMEs, a remarkable seasonal pattern of frontal scale growth is observed between summer and winter. A front-based classification of LMEs is proposed that lends itself to comparison studies of LMEs. Remote sensing of fronts in the World Ocean LMEs appears as a highly effective tool for integrated assessments of physical and biological conditions in LMEs.

Acknowledgments

I.B. and P.C. have been funded by NASA to conduct a global survey of SST fronts from satellite data. I.B. has also been funded by NOAA to study SST fronts in the Alaskan Seas and chlorophyll and SST fronts in the NW Atlantic. I.B.'s travel to the second Global Conference on LMEs was supported by IUCN. Discussions with John O'Reilly were most helpful. David Ullman's assistance in satellite data processing was indispensable. The front detection and cloud masking algorithms were run by Zhengqiang Shan. The original manuscript has been substantially improved thanks to the comments made by three anonymous reviewers and guest editor, Jason Link. We are especially thankful to informal reviewers who greatly contributed to the manuscript improvement, namely John O'Reilly, Sally Adams, George Hunt, Tom Rossby, Richard Thomson, Gary Borstad, and Philip Orton. The OMC software courtesy of Martin Weinelt.

Appendix A. Supplementary data

Supplementary data associated with this article can be found, in the online version, at doi:10.1016/j.pocean.2009.04.015.

References

Acha, E.M., Mianzan, H.W., Guerreroa, R.A., Favero, M., Bava, J., 2004. Marine fronts at the continental shelves of austral South America: Physical and ecological processes. Journal of Marine Systems 44 (1–2), 83–105.

Bakun, A., 1990. Global climate change and intensification of coastal ocean upwelling. Science 247 (4939), 198–201. doi:10.1126/science.247.4939.198.

Belkin, I.M., 2002. Front. In: Nybakken, J.W., Broenkow, W.W., Vallier, T.L. (Eds.), Interdisciplinary Encyclopedia of Marine Sciences. Grolier, Danbury, CT, pp. 433–436.

Belkin, I.M., 2004. Propagation of the "Great Salinity Anomaly" of the 1990s around the northern North Atlantic. Geophysical Research Letters 31, L08306. doi:10.1029/2003GL019334.

Belkin, I.M., 2005. Oceanic fronts in Large Marine Ecosystems. Final Report to the United Nations Environment Programme, 49 pp, 64 maps.

Belkin, I.M., 2009. Rapid warming of Large Marine Ecosystems. Progress in Oceanography, this issue, doi:10.1016/j.pocean.2009.04.011.

Belkin, I.M., Cornillon, P.C., 2003. SST fronts of the Pacific coastal and marginal seas. Pacific Oceanography 1 (2), 90–113.

Belkin, I.M., Cornillon, P.C., 2004. Surface thermal fronts of the Okhotsk Sea. Pacific Oceanography 2 (1–2), 6–19.

Belkin, I.M., Cornillon, P.C., 2005. Bering Sea thermal fronts from Pathfinder data: Seasonal and interannual variability. Pacific Oceanography 3 (1), 6–20.

Belkin, I.M., Cornillon, P.C., 2007. Fronts in the world ocean's Large Marine Ecosystems, ICES CM 2007/D:21, 33 pp.

Belkin, I.M., Cornillon, P., Ullman, D., 2003. Ocean fronts around Alaska from satellite SST data. In: Proceedings of the American Meteorological Society Seventh Conference on the Polar Meteorology and Oceanography, Hyannis, MA, Paper 12.7, 15 pp.

Belkin, I.M., Cornillon, P., Shan, Z., 2001. Global survey of ocean fronts from Pathfinder SST data. Abstracts of the Oceanography Society Meeting, April 2–5, 2001, Miami Beach, FL. Oceanography 14 (1), 10.

Belkin, I.M., Levitus, S., Antonov, J.I., Malmberg, S.-A., 1998a. "Great Salinity Anomalies" in the North Atlantic. Progress in Oceanography 41 (1), 1–68. doi:10.1016/S0079-6611(98)00015-9.

Belkin, I.M., Shan, Z., Cornillon, P., 1998b. Global survey of oceanic fronts from Pathfinder SST and in-situ data. In: Abstracts of the AGU 1998 Fall Meeting. Eos, Transactions of the American Geophysical Union 79 (45, Suppl.), F475.

Cayula, J.-F., Cornillon, P., 1992. Edge detection algorithm for SST images. Journal of Atmospheric and Oceanic Technology 9 (1), 67–80.

Cayula, J.-F., Cornillon, P., 1995. Multi-image edge detection for SST images. Journal of Atmospheric and Oceanic Technology 12 (4), 821–829.

Cayula, J.-F., Cornillon, P., 1996. Cloud detection from a sequence of SST images. Remote Sensing of Environment 55 (1), 80–88.

Cayula, J.-F., Cornillon, P., Holyer, R., Peckinpaugh, S., 1991. Comparative study of two recent edge-detection algorithms designed to process sea-surface temperature fields. IEEE Transactions on Geoscience and Remote Sensing 29 (1), 175–177.

Chen, C.T.A., 2009. Chemical and physical fronts in the Bohai, Yellow and East China Seas. Journal of Marine Systems. doi:10.1016/j.jmarsys.2008.11.016.

Franco, B.C., Piola, A.R., Rivas, A.L., Baldoni, A., Pisoni, J.P., 2008. Multiple thermal fronts near the Patagonian Shelf break. Geophysical Research Letters 35, L02607. doi:10.1029/2007GL032066.

Gentry, R.L., 1998. Behavior and Ecology of the Northern Fur Seal. Princeton University Press, Princeton, NJ. 392 pp.

Glorioso, P.D., Flather, R.A., 1997. The Patagonian Shelf tides. Progress in Oceanography 40 (1–4), 263–284.

Govoni, J.J., Hare, J.A., 2001. The Charleston Gyre as a spawning and larval nursery habitat for fishes. In: Sedberry, G.R. (Ed.), Island in the Stream: Oceanography and Fisheries of the Charleston Bump. American Fisheries Society Symposium 25. American Fisheries Society, Bethesda, MD, pp. 123–136.

Greene, C.H., Pershing, A.J., Cronin, T.M., Ceci, N., 2008. Arctic climate change and its impacts on the ecology of the North Atlantic. Ecology 89 (Suppl. 11), S24–S38.

Haney, J.C., McGillivary, P.A., 1985. Midshelf fronts in the South Atlantic Bight and their influence on seabird distribution and seasonal abundance. Biological Oceanography 3 (4), 401–430.

Hickey, B.M., 1998. Coastal oceanography of western North America from the tip of Baja California to Vancouver Island. In: Robinson, A.R., Brink, K.H. (Eds.), The Sea, vol. 11. Wiley, New York, NY, pp. 345–393.

Hickox, R., Belkin, I.M., Cornillon, P., Shan, Z., 2000. Climatology and seasonal variability of ocean fronts in the East China, Yellow and Bohai Seas from satellite SST data. Geophysical Research Letters 27 (18), 2945–2948.

Huh, O.K., Wiseman Jr., W.J., Rouse Jr., L.J., 1978. Winter cycle of sea surface thermal patterns, northeastern Gulf of Mexico. Journal of Geophysical Research 83 (C9), 4523–4529.

Krause, G., Budeus, G., Gerdes, D., Schaumann, K., Hesse, K., 1986. Frontal systems in the German Bight and their physical and biological effects. In: Nihoul, J.C.J. (Ed.), Marine Interfaces Ecohydrodynamics. Elsevier, Amsterdam, pp. 119–140.

Le Fevre, J., 1986. Aspects of the biology of frontal systems. Advances in Marine Biology 23, 163–299.

Longhurst, A.R., 2006. Ecological Geography of the Sea, second ed. Academic Press, New York, NY. 560 pp.

Lutjeharms, J.R.E., Shillington, F.A., Duncombe Rae, C.M., 1991. Observations of extreme upwelling filaments in the Southeast Atlantic Ocean. Science 253 (5021), 774–776.

Mavor, P.T., Bisagni, J.J., 2001. Seasonal variability of sea-surface temperature fronts on Georges Bank. Deep-Sea Research II 48 (1–3), 215–243.

Merino, M., 1997. Upwelling on the Yukatan Shelf: Hydrographic evidence. Journal of Marine Systems 13 (1–4), 101–121.

Miller, P.I., 2004. Multi-spectral front maps for automatic detection of ocean colour features from SeaWiFS. International Journal of Remote Sensing 25 (7–8), 1437–1442.

Miller, P.I., 2009. Composite front maps for improved visibility of dynamic sea-surface features on cloudy SeaWiFS and AVHRR data. Journal of Marine Systems. doi:10.1016/j.jmarsys.2008.11.019.

Minobe, S., Kuwano-Yoshida, A., Komori, N., Xie, S.-P., Small, R.J., 2008. Influence of the Gulf Stream on the troposphere. Nature 452 (7184), 206–209. doi:10.1038/nature06690.

Nieto, K., Demarcq, H., 2006. Multi-image edge detection on SST and chlorophyll satellite images in northern Chile. In: Report of the Workshop on Indices of Mesoscale Structures (WKIMS), 22–24 February 2006, IFREMER, Nantes, France. ICES WKIMS Report 2006, ICES Oceanography Committee, ICES CM 2006/OCC:01, 48 pp. Available from: <http://www.ices.dk/reports/occ/2006/wkims06.pdf>.

Nielsen, M.H., 2005. The baroclinic surface currents in the Kattegat. Journal of Marine Systems 55 (3–4), 97–121.

NMFS (National Marine Fisheries Service), 1992. Recovery plan for the Steller sea lion (*Eumetopias jubatus*). Prepared by the Steller Sea Lion Recovery Team for the National Marine Fisheries Service, Silver Spring, MD, 92 pp.

Olson, D.B., Hitchcock, G.L., Mariano, A.J., Ashjan, C.J., Peng, G., Nero, R.W., Podesta, G.P., 1994. Life on the edge: marine life and fronts. Oceanography 7 (2), 52–60.

Omstedt, A., Elken, J., Lehmann, A., Piechura, J., 2004. Knowledge of the Baltic Sea physics gained during the BALTEX and related programmes. Progress in Oceanography 63 (1–2), 1–28.

Otto, L., Zimmerman, J.T.F., Furnes, G.K., Mork, M., Saetre, R., Becker, G., 1990. Review of the physical oceanography of the North Sea. Netherlands Journal of Sea Research 26 (2–4), 161–238.

Perez, R., Müller-Karger, F.E., Victoria, I., Melo, N., Cerdeira, S., 1999. Cuban, Mexican, US researchers probing mysteries of Yucatan Current. Eos, Transactions of the American Geophysical Union 80(14), 153, 158.

Pinchuk, A.I., Paul, A.J., 2000. Zooplankton of the Okhotsk Sea: A review of Russian studies. University of Alaska Sea Grant, AK-SG-00-02, Fairbanks, AK, 62 pp.

Rivas, A.L., 2006. Quantitative estimation of the influence of surface thermal fronts over chlorophyll concentration at the Patagonian Shelf. Journal of Marine Systems 63 (3–4), 183–190.

Sedberry, G.R., McGovern, J.C., Pashuk, O., 2001. The Charleston Bump: an island of essential fish habitat in the Gulf Stream. In: Sedberry, G.R. (Ed.), Island in the Stream: Oceanography and Fisheries of the Charleston Bump. American Fisheries Society Symposium 25. American Fisheries Society, Bethesda, MD, pp. 3–24.

Sherman, K., 1990. Productivity, perturbations, and options for biomass yields in large marine ecosystems. In: Sherman, K., Alexander, L.M., Gold, B.D. (Eds.), Large Marine Ecosystems: Patterns, Processes and Yields. AAAS Publications, Washington, DC, pp. 206–219.

Sherman, K., 2005. The large marine ecosystem approach for assessment and management of ocean coastal waters. In: Hennessey, T., Sutinen, J. (Eds.), Sustaining the Large Marine Ecosystem: The Human Dimension. Elsevier, Amsterdam, pp. 3–16.

Sherman, K., Belkin, I.M., Friedland, K.D., O'Reilly, J., Hyde, K., 2009. Accelerated warming and emergent trends in fisheries biomass yields of the world's Large Marine Ecosystems. AMBIO, in press.

Small, R.J., deSzoeke, S.P., Xie, S.P., O'Neill, L., Seo, H., Song, Q., Cornillon, P., Spall, M., Minobe, S., 2008. Air–sea interaction over ocean fronts and eddies. Dynamics of Atmospheres and Oceans 45 (3–4), 274–319.

Ullman, D.S., Cornillon, P.C., 1999. Surface temperature fronts off the East Coast of North America from AVHRR imagery. Journal of Geophysical Research 104 (C10), 23459–23478.

Ullman, D.S., Cornillon, P.C., 2000. Evaluation of front detection methods for satellite-derived SST data using in situ observations. Journal of Atmospheric and Oceanic Technology 17 (12), 1667–1675.

Ullman, D.S., Cornillon, P.C., 2001. Continental Shelf surface thermal fronts in winter off the northeast US coast. Continental Shelf Research 21 (11–12), 1139–1156.

Vazquez, J., Perry, K., Kilpatrick, K., 1998. NOAA/NASA AVHRR Oceans Pathfinder Sea Surface Temperature Data Set User's Reference Manual, Version 4.0, JPL Publication D-14070. Available from: <http://podaac.jpl.nasa.gov/pub/sea_surface_temperature/avhrr/pathfinder/doc/usr_gde4_0.html>.